Supporting Information

1. Experimental section

1.1 Materials and synthesis

***General information*:** (4,8-bis(5-(2-ethylhexyl)thiophen-2-yl)benzo[1,2-b:4,5-b']dithiophene-2,6-diyl)bis(trimethylstannane) (BDT-TH) and (4,8-bis(5-(2-ethylhexyl)-4-fluorothiophen-2-yl)benzo[1,2-b:4,5-b']dithiophene-2,6-diyl)bis(trimethylstannane) (BDT-TF) were purchased from Suna Tech Inc. The catalyst and ligand were purchased from Strem Chemical, Inc and Sinopharm Chemical Reagent Co., Ltd, respectively. Other reagents were purchased from Energy Chemical (Sun Chemical Technology (Shanghai) Co., Ltd.) or Bide Pharmatech Ltd. Unless otherwise stated, analytical grade solvents and commercially available reagents were used without further purification. Chromatography columns were packed with 200-300 mesh silica gel in petroleum ether (bp. 60 - 90 ºC). All new compounds were characterized by ^{1}H NMR and ^{13}C NMR spectra, which were recorded on an AVANCE NEO 600 MHz spectrometer at room temperature. The chemical shifts (δ) were given in part per million relatives to internal tetramethyl silane (TMS, 0 ppm for ^{1}H) and $CDCl_3$ (77.0 ppm for ^{13}C). All chemical shifts (δ) were reported in ppm and coupling constants (*J*) in Hz. High-resolution mass spectrum (MALDI-TOF-MS) was determined using an autoflex max TOF Mass Spectrometer, peaks are given in m/z. The molecular weight of the polymers was estimated by high-temperature gel permeation chromatography (HT-GPC) using 1,2,4-trichlorobenzene (TCB) as the eluent at 160 ℃ and monodispersed polystyrene as the standard. The configuration optimizations of the three polymers were conducted by Density functional theory (DFT) calculations using the Gaussian 16 program[1] at the B3LYP/6-31G (d, p) level of theory on the neutral model molecules of each polymer. All of the long alkyl chains have been replaced by methyl groups for simplification.

Synthesis of compound 1: 3-octyl-thiophene (1.765 g, 8.99 mmol) was added to a dried 250 mL flask under a nitrogen atmosphere. Subsequently, 80 mL of tetrahydrofuran (THF) was added. After the solution was cooled to -78 ℃, *n*-butyllithium (2.5M in THF, 3.6 mL, 8.99 mmol) was added slowly. After 3.5 mL dimethylformamide (DMF) was added via syringe, this mixture was stirred for 2 h at -78 ℃ and warmed to room temperature, and the reaction was stirred overnight. Volatile solvents were removed under a vacuum, and the residue was partitioned between petroleum ether (PE) and brine. The layers were separated, and the aqueous phase was washed once with PE. The combined organic phase was washed once with brine, dried over $MgSO_4$, filtered, and concentrated under a vacuum to obtain a crude product. Finally, the crude product was purified by silica gel chromatography to obtain 1.797 g of compound 1 as a yellow oil with a yield of 89% (PE/dichloromethane (DCM) = 5/1, v/v). ^{1}H NMR (600 MHz, $CDCl_3$, δ/ppm) 9.87 (s, 1H), 7.60 (s, 1H), 7.37 (s, 1H), 2.63 (t, J = 7.8 Hz, 2H), 1.65-1.62 (m, 2H), 1.30-1.26 (m, 10H), 0.88 (t, J = 7.2 Hz, 3H). ^{13}C NMR (151 MHz, $CDCl_3$, δ/ppm) 183.06, 144.80, 143.60, 137.19, 130.46, 31.86, 30.42, 30.15, 29.37, 29.23, 29.17, 22.67, 14.12.

Synthesis of compound 2: Compound1 (0.400 g, 1.78 mmol), S_8 (0.057 g, 0.23 mmol), 1-methylpyrrolidine-2,5-dione (0.096 g, 0.85 mmol), 2-aminobenzimidazole (0.118 g, 0.89 mmol), NH_4I (0.142 g, 0.98 mmol), K_2CO_3 (0.135 g, 0.98 mmol), N-methyl-2-pyrrolidone (2.0 mL), and H_2O (0.2 mL) were added to a 10 mL reaction vessel. The mixture was charged at 140 ℃ in an oil bath for 48 h. After cooling to room temperature, the reaction was extracted with DCM and then washed with brine, dried over $MgSO_4$, filtered, and concentrated under a vacuum to obtain a crude product. The residue was purified by silica gel chromatography (PE/DCM, v/v = 2:1) as eluent to yield the desired compound 2 as a yellow solid (0.207 g, 42% yield). ^{1}H NMR (600 MHz, $CDCl_3$, δ/ppm) δ 7.78 (s, 2H), 7.03 (s, 2H), 3.17 (s, 3H), 2.63 (t, J = 7.8 Hz, 4H), 1.66-1.64 (m, 4H), 1.35-1.27 (m, 20H), 0.89 (t, J = 7.2 Hz, 6H). ^{13}C NMR (151 MHz, $CDCl_3$, δ/ppm) 162.76, 144.95, 136.92, 132.11, 131.08, 127.95, 123.62, 31.88, 30.45, 30.41, 29.40, 29.30, 29.27, 24.34, 22.68, 14.12.

Synthesis of compound 3: N-bromosuccinimide (NBS, 0.162 g, 2.84 mmol) was added to the solution containing 30 mL chloroform (CF), 20 mL of acetic acid (HOAc), and compound 2 (0.752 g, 1.35 mmol) under ice bath. After the ice was naturally melted, the mixture was stirred at room temperature under the dark for one night. Then the mixture was washed with sodium bicarbonate solution, extracted with DCM (3 x 30 mL), and dried over $MgSO_4$. The solvent was removed by a rotate evaporator and the residue was purified by silica gel chromatography (PE/DCM = 4/1, v/v) to yield compound 3 as a yellow solid (0.791 g, yield 82%). ^{1}H NMR (600 MHz, $CDCl_3$, δ/ppm) 7.61 (s, 2H), 3.13 (s, 3H), 2.55 (t, *J* = 8.7 Hz, 4H), 1.62-1.60 (m, 4H), 1.34-1.28 (m, 20H), 0.89 (t, *J* = 6.9 Hz, 6H). ^{13}C NMR (151 MHz, $CDCl_3$, δ/ppm) 162.45, 162.42, 143.77, 135.55, 135.53, 135.52, 131.83, 130.29, 128.19, 128.17, 113.59, 31.89, 29.63, 29.52, 29.36, 29.27, 24.40, 22.69, 14.14. MS (MALDI-TOF) m/z Calcd. For $C_{31}H_{39}Br_2NO_2S_3$: 714.056, Found 714.016.

Polymerization of PTTB-X: To a mixture of BDT-TX (0.100 mmol), compound 3 (76.0 mg, 0.100 mmol), $Pd_2(dba)_3$ (4.0 mg, 0.004 mmol), and P(o-Tol)$_3$ (10.0 mg, 0.035 mmol) in a Schlenk flask was added chlorobenzene (3 mL) under argon. The mixture was reacted at 120 °C for 14 h. Then the solution was cooled to 60 °C and precipitated in 30 mL methanol. The precipitate was collected and further purified via Soxhlet extraction by using methanol, acetone, DCM, DCM:CF (1:1,v/v), and CF in sequence. The CF fraction was concentrated under reduced pressure and precipitated in methanol to obtain the resulting polymer as a dark solid.

PTTB-H: 101.6 mg (82.2%), M_n: 25.0 kDa with a PDI of 2.14.

PTTB-F: 98.7 mg (75.4%), M_n: 26.3 kDa with a PDI of 2.35.

1.2 Characterization of photovoltaic materials

Device Fabrication and Testing: All the devices were fabricated with a conventional structure architecture of Glass/ITO (Indium tin oxide)/ poly(3,4-ethylenedioxythiophene): poly(styrene sulfonate) (PEDOT: PSS) /Active layer/ poly[(9,9-bis(3′-((N, N-dimethyl)-Nethylammonium)propyl)-2,7-fluorene)-alt-5,5′-

bis(2,2′-thiophene)-2,6-naphthalene-1,4,5,8-tetracarboxylic-N,N′-di(2-ethylhexyl)imide]dibromide (PNDIT-F3N-Br)/Ag, in which L8-BO was used as electron acceptor and PEDOT: PSS and PNDIT-F3N-Br served as anode and cathode buffer layers, respectively. Pre-patterned ITO-coated glass substrates (purchased from South China Science & Technology Company Limited) washed with methylbenzene, deionized water, acetone, and isopropyl alcohol in an ultrasonic bath for 15 minutes each. After blow-drying with high-purity nitrogen, all ITO substrates are cleaned in the ultraviolet ozone cleaning system for 15 minutes. A thin layer of PEDOT: PSS (40 nm) was deposited through spin-coating on precleaned ITO-coated glass from a PEDOT: PSS aqueous solution (Xi'an Polymer Light Technology Corp 4083) at 3000 rpm for 30 s and dried subsequently at 150 °C for 15 minutes in atmospheric air. Then the active layers were spin-coated from $CHCl_3$ solution with the same optimal donor/acceptor weight ratios of 1:1.2 with a total concentration of 17 mg mL^{-1}, which were further annealed at 110 ℃ for 3 min. A PNDIT-F3N-Br layer via a solution concentration of 1.0 mg mL^{-1} was deposited on the top of the active layer at a rate of 3000 rpm for 30 s. Finally, the top silver electrode of 100 nm thickness was thermally evaporated through a mask onto the cathode buffer layer under a vacuum of$\sim 5\times10^{-6}$ mbar. The optimal active layer thickness measured by a Bruker Dektak XT stylus profilometer was about 110 nm. The typical active area of the investigated devices was 5 mm^2. The current-voltage characteristics of the solar cells were measured by a Keithley 2400 source meter unit under AM1.5G (100 mW cm^{-2}) irradiation from a solar simulator (Enlitech model SS-F5-3A). Solar simulator illumination intensity was determined at 100 mW cm^{-2} using a monocrystalline silicon reference cell with a KG5 filter. Short circuit currents under AM1.5G (100 mW cm^{-2}) conditions were estimated from the spectral response and convolution with the solar spectrum. The external quantum efficiency was measured by a Solar Cell Spectral Response Measurement System QE-R3011(Enli Technology Co., Ltd.).

1.3 Instruments and Characterization

Ultraviolet-visible near-infrared (UV-vis-NIR) absorption measurements: UV-vis-

NIR absorption spectra were recorded with a Perkin-Elmer Lambda 365 UV-vis spectrophotometer from 300 nm to 1100 nm.

Cyclic voltammetry (CV) measurements: Electrochemical properties were studied by CV, which was performed on a CS350H electrochemical workstation with a conventional three-electrode system in a tetrabutylammonium hexafluorophosphate (*n*-Bu_4NPF_6, 0.1 M) acetonitrile solution at a scan rate of 100 mV s^{-1}. A glassy carbon disc coated with sample film was used as the working electrode. A Pt wire was used as the counter electrode, and Ag/AgCl was used as the reference electrode. The HOMO and LUMO energy levels (E_{HOMO}/E_{LUMO}) can be calculated from the onset oxidation/reduction potentials (E_{ox}/E_{red}) in the cyclic voltammograms according to the equations of $E_{HOMO}/E_{LUMO} = -(E_{ox}/E_{red} + 4.8 - E_{Fc}/_{Fc}^{+})$ (eV), where $E_{Fc}/_{Fc}^{+}$ is the redox potential of ferrocene/ferrocenium (Fc/Fc^+) couple in the electrochemical measurement system, and the energy level of Fc/Fc^+ was taken as -4.8 eV below the vacuum level.

Space charge limited current (SCLC) measurements: Single carrier devices were fabricated and the dark current-voltage characteristics were measured and analyzed in the space charge limited (SCL) regime following the references. The structure of hole-only devices was Glass/ITO/PEDOT: PSS/Active layer/MoO_3/Ag. For the electron-only devices, the structure was Glass/ITO/ZnO/Active layer/PNDIT-F3N-Br/Ag, where Ag was evaporated. The reported mobility data are average values over the two cells of each sample at a given film composition. The device characteristics were extracted by modeling the dark current under forward bias using SCLC expression described by Mott-Gurney law: $J = \frac{9}{8}\varepsilon_r\varepsilon_0\,\mu\frac{V^2}{L^3}$. Here, ε_r is the average dielectric constant of the blend film, ε_0 is the permittivity of the free space, μ is the carrier mobility, $L\approx100$ nm is the thickness of the film, and V is the applied voltage.

Photoluminescence (PL)measurements. The PL data and emission of relevant films were collected using a Zolix Flex One Spectrometer. The PL excitation wavelength was set to 639 nm.

Transient photocurrent (TPC) measurements: Relevant solar cells were excited with

a 405 nm laser diode. The transient photocurrent response of the devices at short circuit condition to a 200 μs square pulse from the LED with no background illumination. The current traces were recorded on a Tektronix DPO3034 digital oscilloscope by measuring the voltage drop over a 5-ohm sensor resistor in series with the solar cell. DC voltage was applied to the solar cell with an MRF544 bipolar junction transistor in a common collector amplifier configuration.

Transient photovoltage (TPV) measurements: A 405 nm laser diode was used to keep the organic solar cells in the V_{OC} conditions. Measuring the light intensity with a highly linear photodiode and driving the laser intensity with a waveform generator (Agilent 33500B). Moreover, a small perturbation was induced with a second 405 nm laser diode. The intensity of the short laser pulse was adjusted to keep the voltage perturbation below 10 mV. After the pulse, the voltage decays back to its steady state value in a single exponential decay.

Contact Angle Measurements and Interfacial Tension Calculation: The contact angles of the active materials were measured using a Contact Angle Analyzer. The contact angles of different solvents (water and ethylene glycol (EG)) on the neat films were used to calculate the surface tension of each film by the Owens-Wendt method.

Atomic force microscopy (AFM) measurements: AFM images were obtained by using a Nano Wizard 4 atomic force microscopy (JPK Inc. Germany) in Qi mode to observe the surface morphologies of the films deposited on glass substrates. The root-mean-square (RMS) roughness values of the surface AFM images are averaged based on five times testing on different areas for each sample.

Transmission electron microscopy (TEM) measurements were carried out using a 200 kV (JEOL ARM-200F). Samples for TEM were prepared on a Cu mesh grid.

Grazing incidence wide-angle X-ray scattering (GIWAXS) characterization: GIWAXS measurements were carried out with a Xeuss 2.0 SAXS/WAXS laboratory beamline using a Cu Kα X-ray source (8.05 keV, 1.54 A) and a Pilatus3R 300 K detector. The incidence angle is 0.2°.

2. Supplemental Figures and Tables

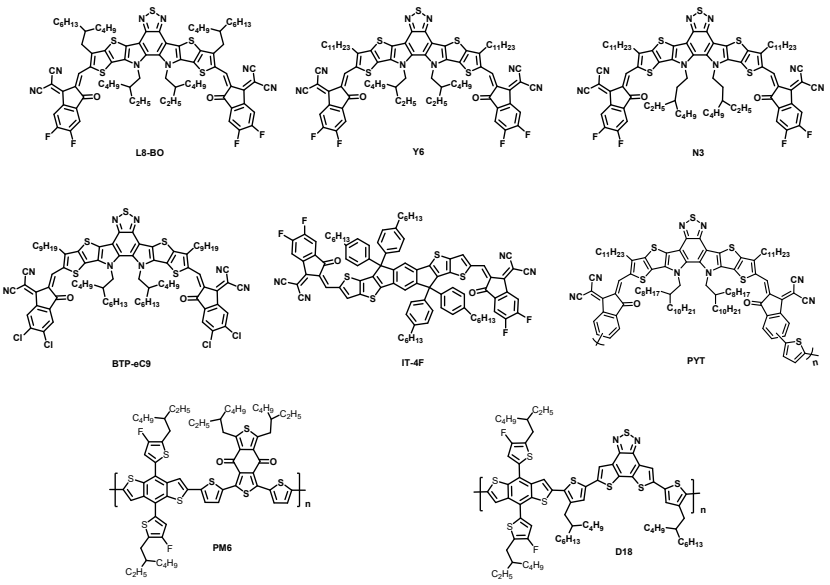

Figure S1. The molecular structures of the investigated materials in this work.

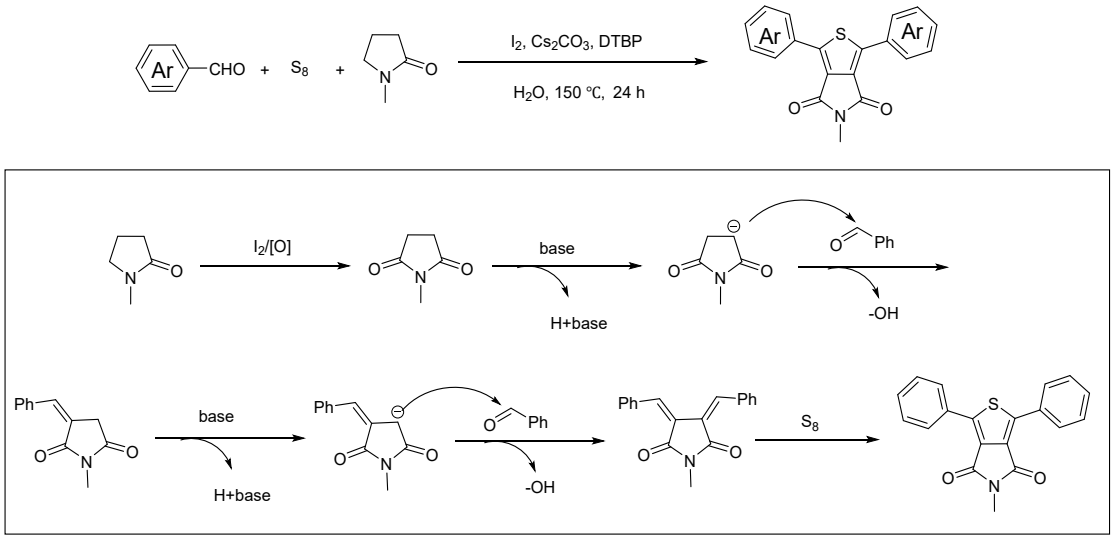

Figure S2. The π−TPD−π derivatives synthesis method developed by Deng *et al.*[2] and its proposed mechanism.

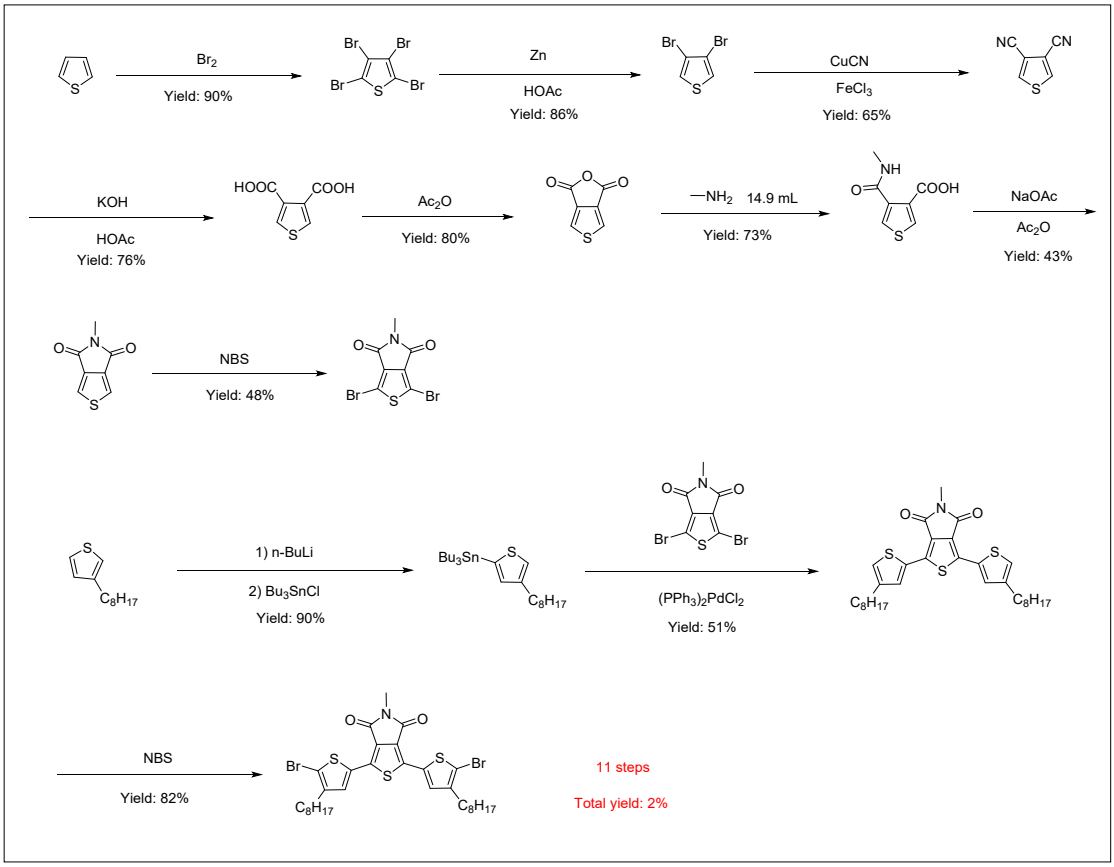

Scheme S1. Detailed synthetic route of compound 3 in the conventional method and the yield of each step.

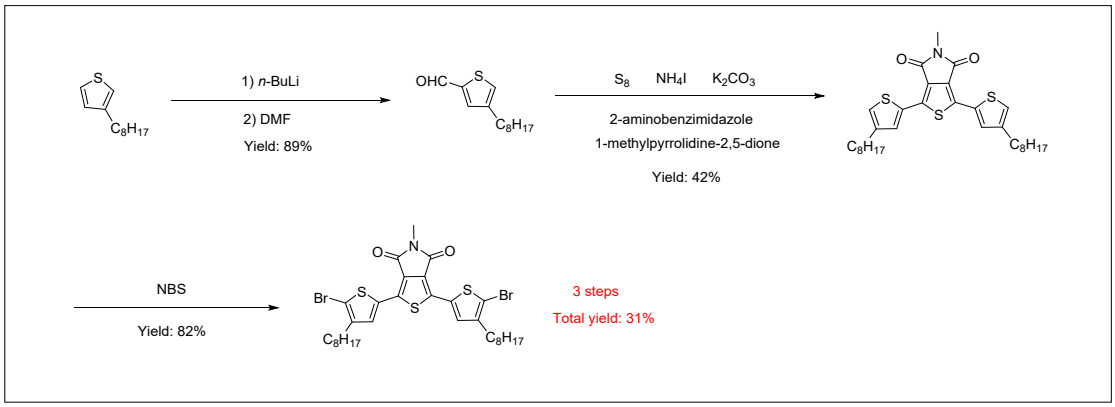

Scheme S2. Detailed synthetic route of compound 3 in this work and the yield of each step.

Table S1. Starting materials, number of synthetic steps (NSS), reciprocal yield (RY), number of operation units for the isolation/purification (NUO), number of column chromatographies for the isolation/purification (NCC) and number of hazardous chemicals (NHC) for traditional and this work synthetic route.[7] The codes of the unit operations are: 1) Quenching/neutralization; 2) Extraction; 3) Column chromatography; 4) Recrystallization; 5) Distillation/sublimation.

Synthetic method	NSS	RY	NUO	NCC	NHC	SC index[a] (%)
Traditional	11	2%	18	4	14	159
This work	3	31%	6	3	1	52

[a] $SC = 35 \times \frac{NSS}{NSSmax} + 25 \times \frac{log(RY)}{log(RYmax)} + 15 \times \frac{NUO}{NUOmax} + 15 \times \frac{NCC}{NCCmax} + 10 \times \frac{NHC}{NHCmax}$

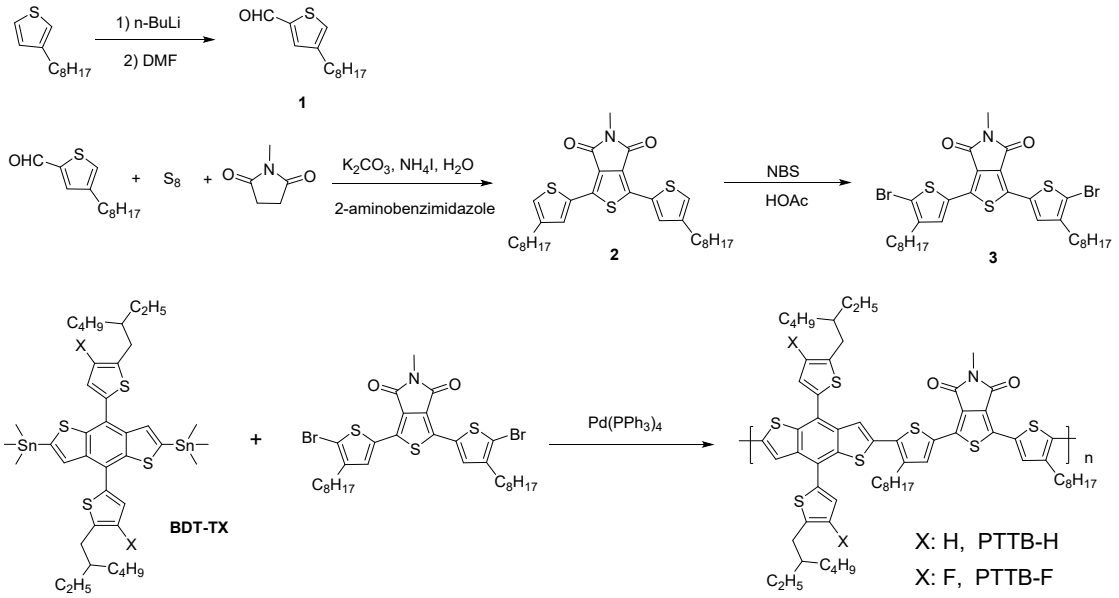

Scheme S3. Synthetic routes of PTTB-H and PTTB-F.

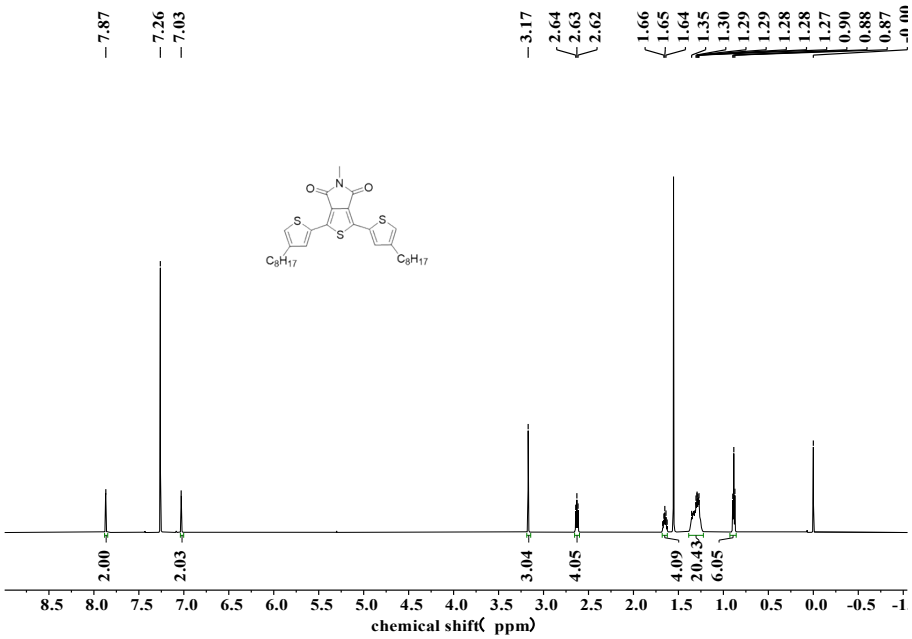

Figure S3. ^{1}H NMR spectrum of compound 2.

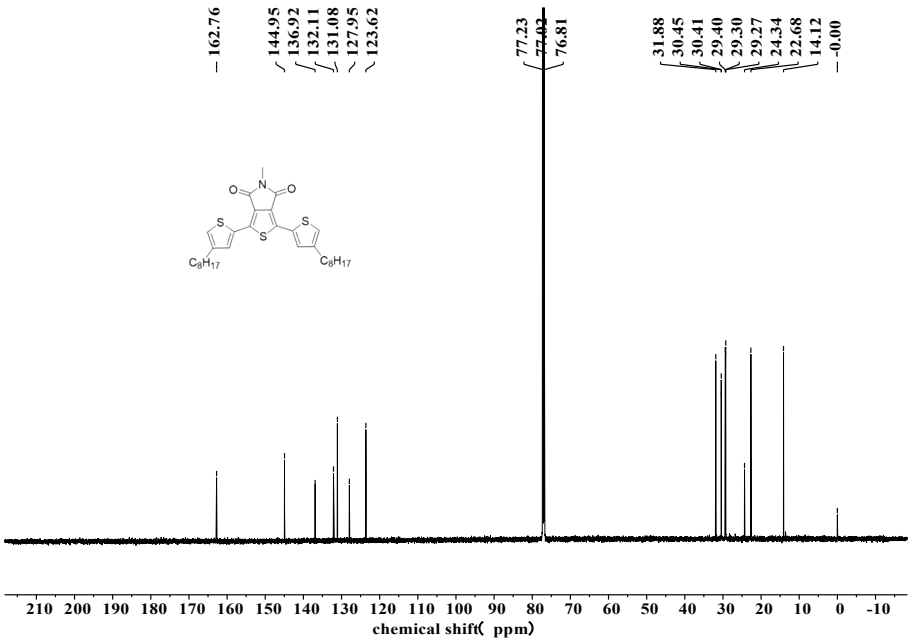

Figure S4. ^{13}C NMR spectrum of compound 2.

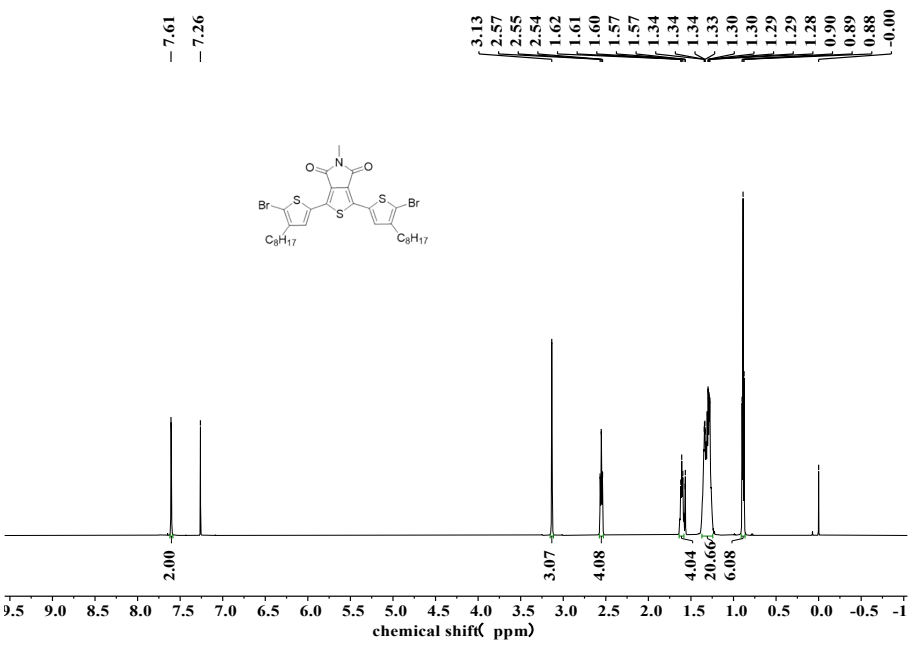

Figure S5. ^{1}H NMR spectrum of compound 3.

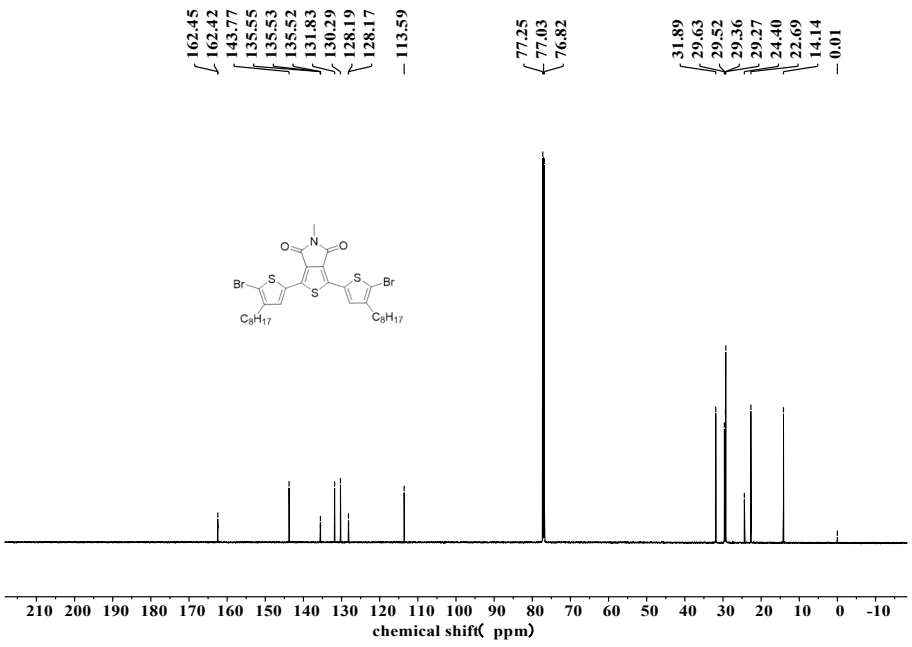

Figure S6. ^{13}C NMR spectrum of compound 3.

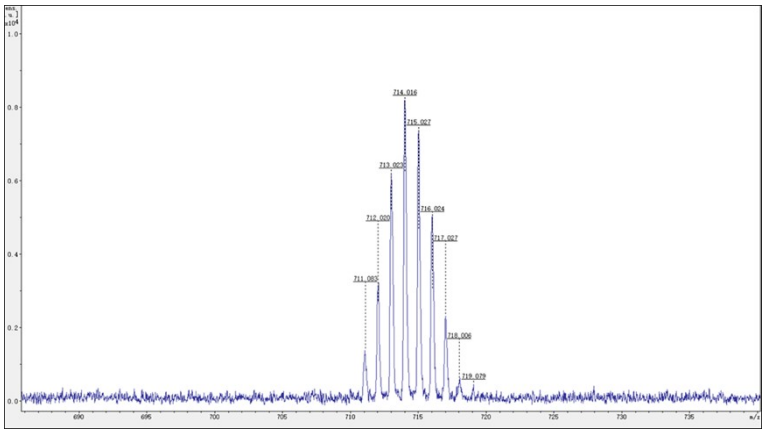

Figure S7. MALDI-TOF spectrum of compound 3.

Table S2. GPC, electrochemical and optical parameters of PTTB-H and PTTB-F.

Polymer	$\bar{M}_n$ [kDa]	PDI	E_{HOMO} [eV]	E_{LUMO}[a] [eV]	λ_{max} [nm]		E_g^{opt} [eV]
					Solution	Film	
PTTB-H	25.0	2.15	-5.33	-3.46	562	560	1.85
PTTB-F	26.3	2.35	-5.56	-3.70	571	565	1.86

[a] $E_{LUMO} = E_{HOMO} + E_g^{opt}$, $E_g^{opt} = 1240/\lambda_{edge}$.

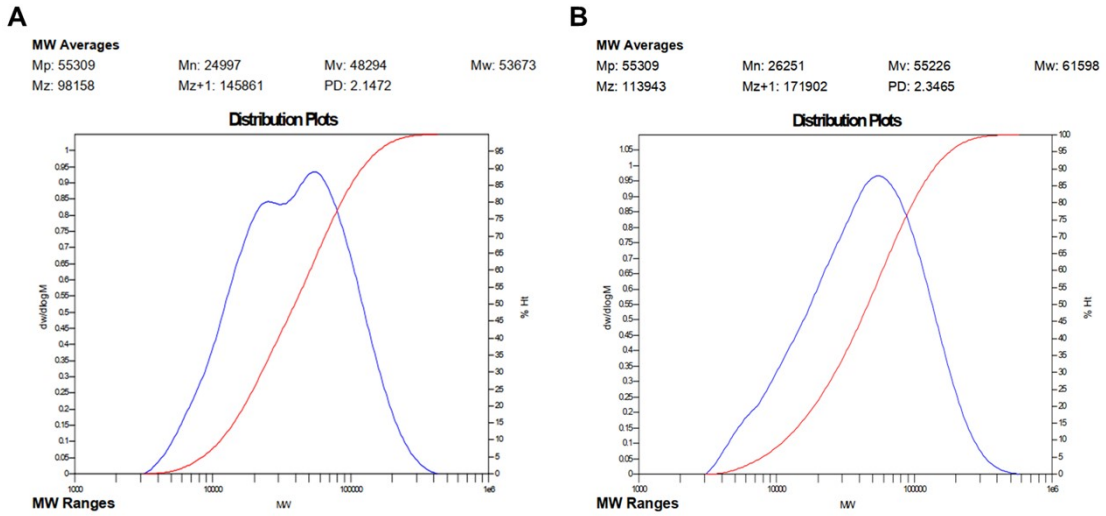

Figure S8. The GPC curves of (A) PTTB-H and (B) PTTB-F polymers.

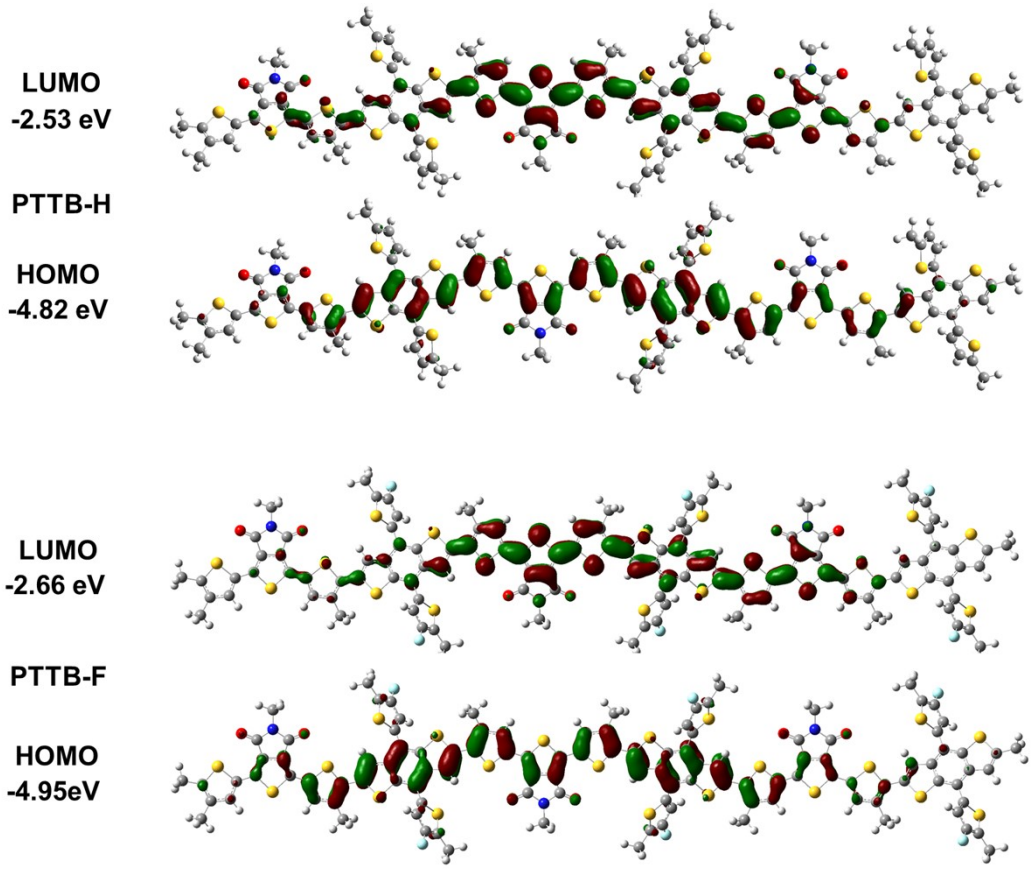

Figure S9. LUMO and HOMO energy levels of PTTB-H and PTTB-F calculated by B3LYP/6-31G (d, p) with methyl groups in replacing alkyl substituents to simplify the calculations.

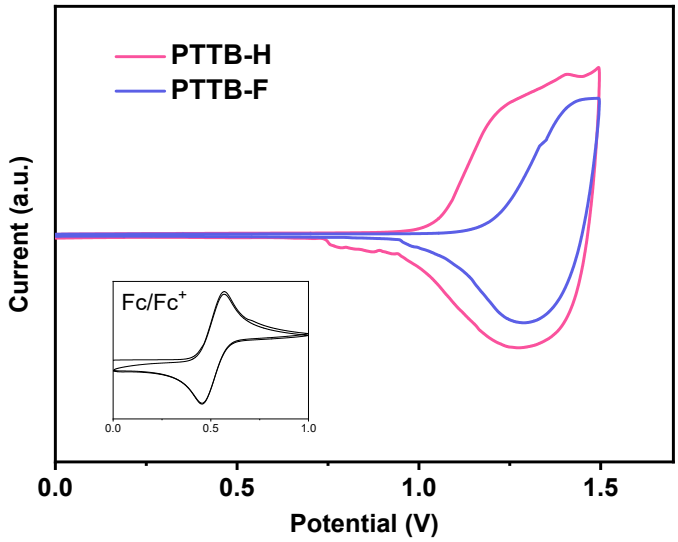

Figure S10. Cyclic voltammogram of PTTB-H, PTTB-F and Fc/Fc^{+}.

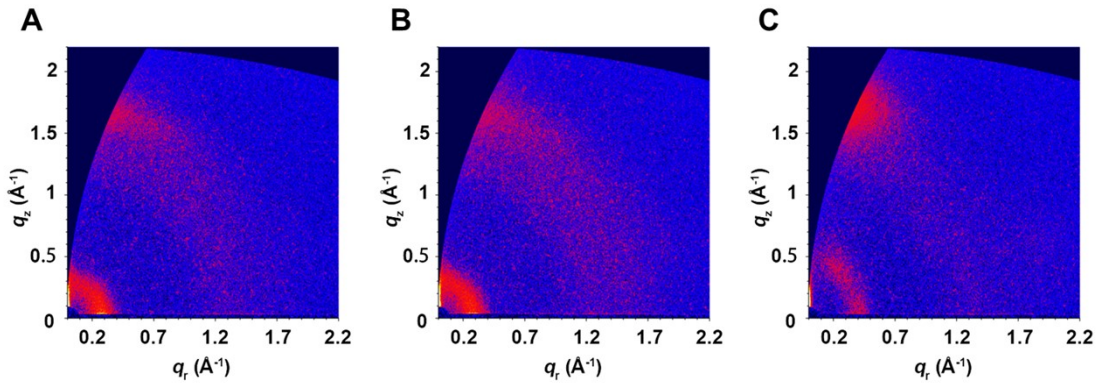

Figure S11. 2D GIWAXS patterns of (A) PTTB-H, (B) PTTB-F and (C) L8-BO films.

Table S3. Investigations of the morphology parameters extracted from the GIWAXS measurements of the pristine and blend films.

Sample	in-plane (100)			out-of-plane (010)		
	location [Å^{-1}]	*d*-spacing [Å]	CCL [Å]	location [Å^{-1}]	*d*-spacing [Å]	CCL [Å]
PTTB-H	0.27	23.6	35.8	1.69	3.72	18.9
PTTB-F	0.27	23.4	38.2	1.70	3.70	23.1
L8-BO	0.41	15.3	38.4	1.75	3.59	17.8
PTTB-H: L8-BO	0.30	20.6	30.7	1.72	3.65	21.5
PTTB-F: L8-BO	0.30	20.6	42.0	1.73	3.64	22.8

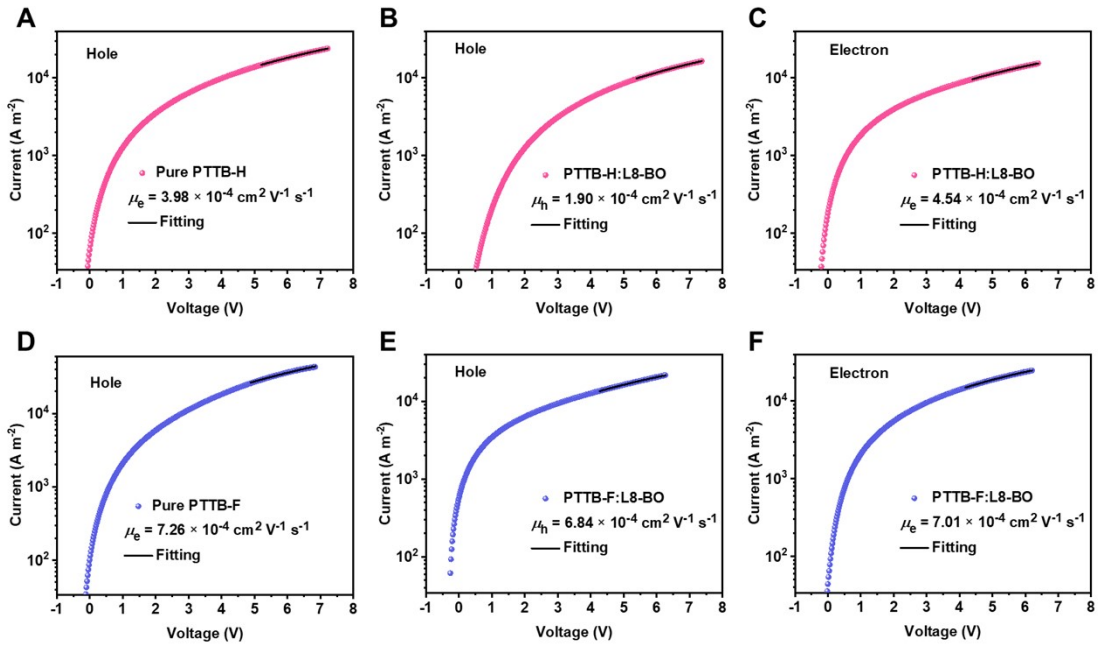

Figure S12. The dark *J-V* characteristics of hole-only and electron-only devices for the (A) PTTB-H and (D) PTTB-F neat films, (B, C) PTTB-H: L8-BO and (E, F) PTTB-F: L8-BO blend films.

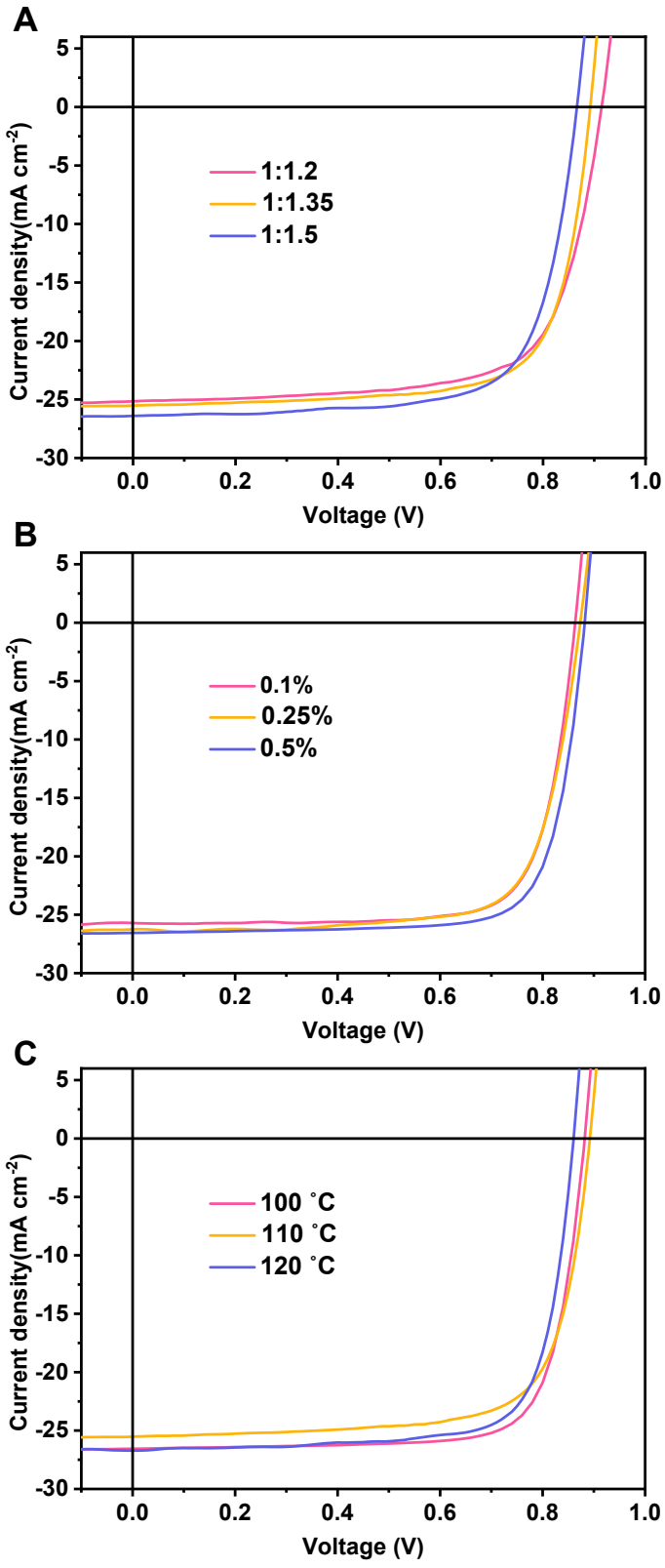

Figure S13. *J-V* curve characteristics of the PTTB-F: L8-BO fabricated with different processing conditions of (A) D/A ratios, (B) 1,8-diiodooctane (DIO) ratios, and (C) thermal-annealing (TA) time, measured under the illumination of AM 1.5G at 100 mW cm^{-2}.

Table S4. Photovoltaic parameters of the PTTB-F: L8-BO devices fabricated with the different donor: acceptor weight ratios, measured under the illumination of AM 1.5G at 100 mW cm^{-2}.

D:A	V_{OC} (V)	J_{SC} (mA cm^{-2})	FF (%)	PCE (%)
1:1.2	0.914	25.16	70.64	16.24
1:1.35	0.892	25.52	73.04	16.63
1:1.5	0.866	26.40	72.25	16.52

Table S5. Photovoltaic parameters of the PTTB-F: L8-BO devices fabricated with different DIO ratios, measured under the illumination of AM 1.5G at 100 mW cm^{-2}.

DIO (%)	V_{OC} (V)	J_{SC} (mA cm^{-2})	FF (%)	PCE (%)
0.1	0.873	26.25	74.15	16.99
0.25	0.882	26.56	77.08	18.06
0.5	0.863	25.71	76.87	17.06

Table S6. Photovoltaic parameters of the PTTB-F: L8-BO devices fabricated with different thermal-annealing temperatures, measured under the illumination of AM 1.5G at 100 mW cm^{-2}.

Temperature (°C)	V_{OC} (V)	J_{SC} (mA cm^{-2})	FF (%)	PCE (%)
100	0.892	25.52	73.04	16.63
110	0.882	26.56	77.08	18.06
120	0.860	26.71	75.34	17.31

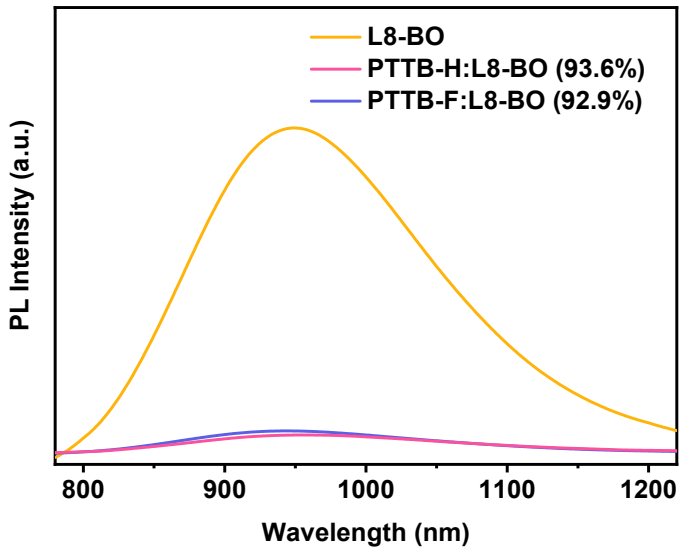

Figure S14. Steady-state PL spectra of the neat L8-BO film and the PTTB-H: L8-BO and PTTB-F: L8-BO blend films.

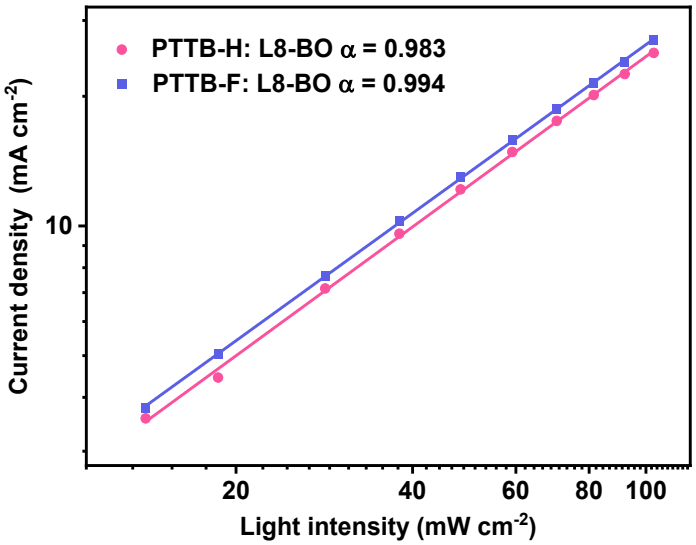

Figure S15. J_{SC} *versus* light intensity curves of the PTTB-H: L8-BO and PTTB-F: L8-BO devices.

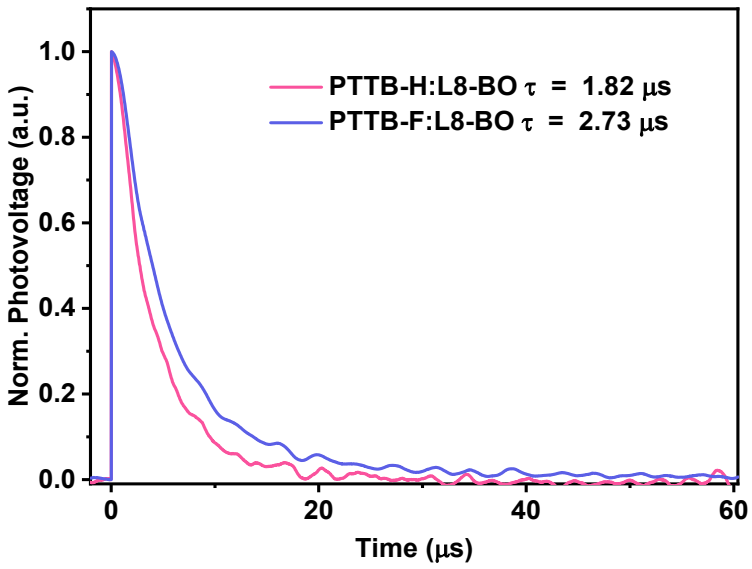

Figure S16. Normalized transient photovoltage data for the PTTB-H: L8-BO and PTTB-F: L8-BO devices.

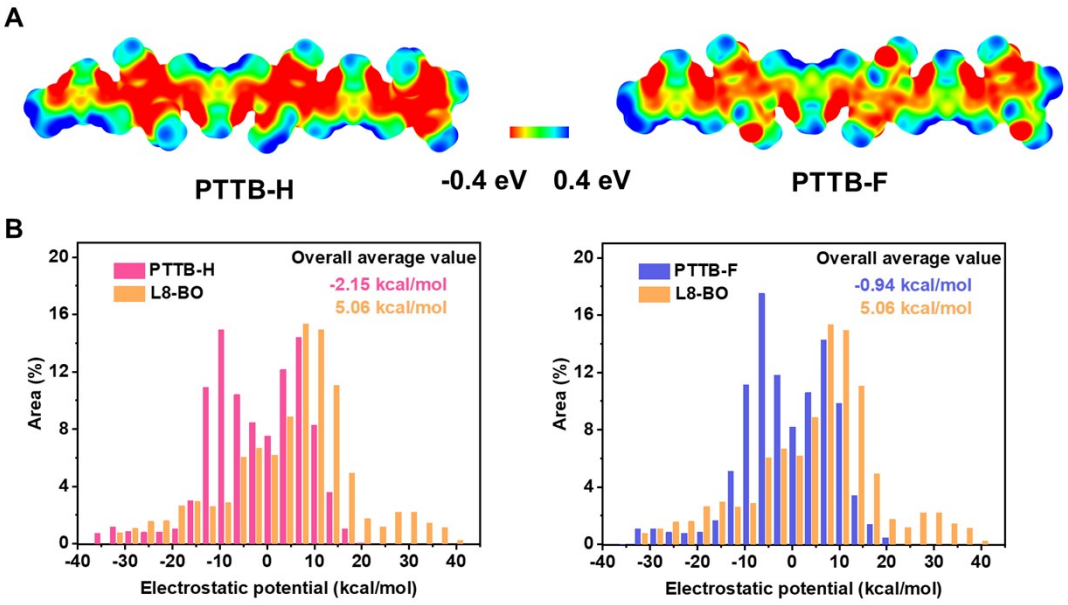

Figure S17. (A) ESP distributions[8] of PTTB-H and PTTB-F. (B) ESP area distributions of the corresponding molecules.

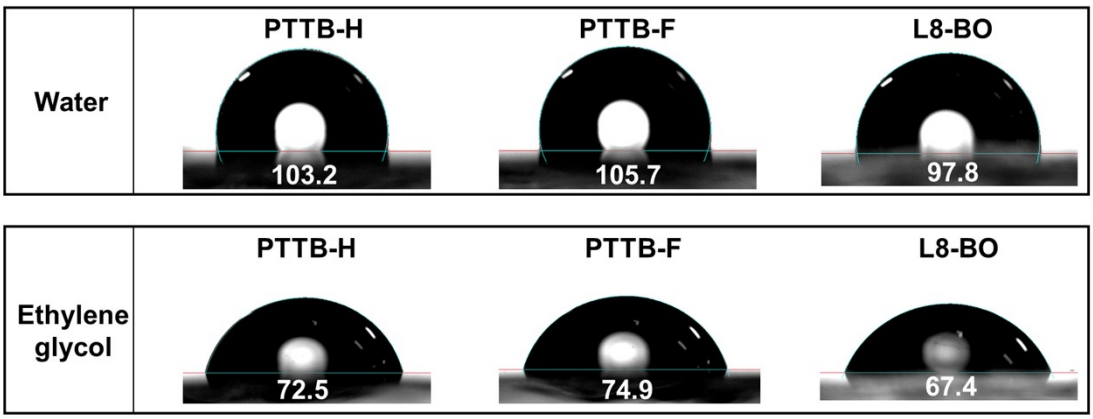

Figure S18. Photographs of water and ethylene glycol droplets on the top surfaces of PTTB-H, PTTB-F, and L8-BO. The contact angle measurement is conducted at the center of the substrates, avoiding the edges of the ITO anodes.

Table S7. Surface tension values of the corresponding neat films, and χ values between the donors and L8-BO.

Sample	Contact		Surface energy (mN m^{-1})	Relative χ
	Water	Ethylene glycol		(With L8-BO)
PTTB-H	103.2±0.06	72.5±0.05	51.97±0.07	0.06 *K*
PTTB-F	105.7±0.04	74.9±0.04	53.32±0.09	0.11 *K*
L8-BO	97.8±0.03	67.4±0.05	48.55±0.06	/

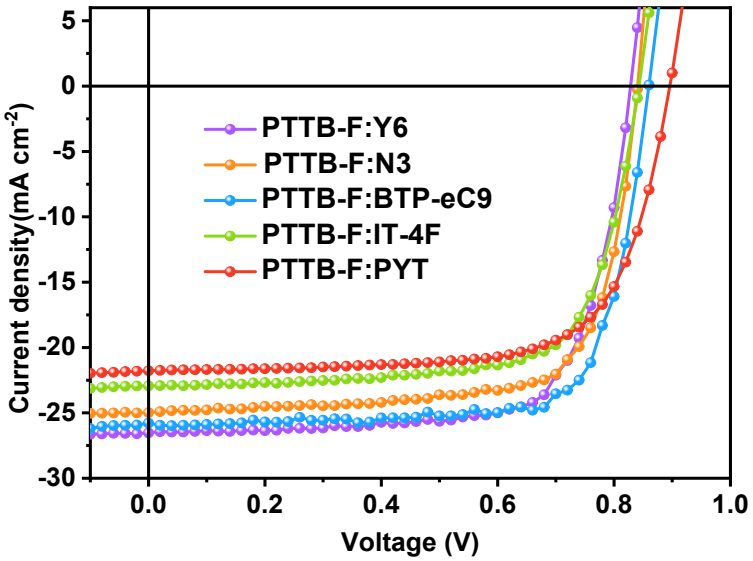

Figure S19. *J-V* curve characteristics of the PTTB-F-based devices blended with various classical small molecule acceptors.

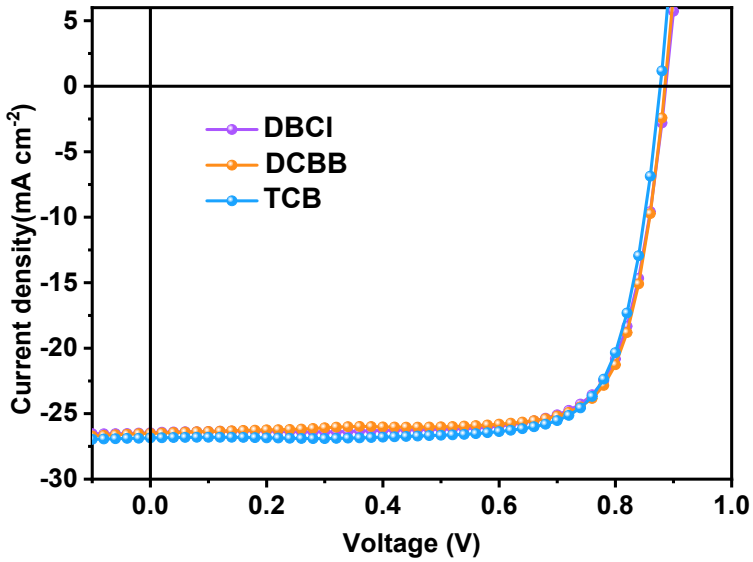

Figure S20. *J-V* curve characteristics of the PTTB-F-based devices fabricated with 1,3-dibromo-5-chlorobenzene (DBCl), 1-bromo-3,5-dichlorobenzene (DCBB), and 1,3,5-trichlorobenzene (TCB) as solid additives.

Table S8. Photovoltaic parameters of the PTTB-F:L8-BO devices fabricated with 1,3-dibromo-5-chlorobenzene (DBCl), 1-bromo-3,5-dichlorobenzene (DCBB), and 1,3,5-trichlorobenzene (TCB) as solid additives under the illumination of AM 1.5G at 100 mW cm^{-2}.

Additives	V_{OC} (V)	J_{SC} (mA cm^{-2})	FF (%)	PCE (PCE)[a] (%)
DBCl	0.887	26.45	76.58	17.97 (17.85±0.10)
DCBB	0.885	26.50	77.26	18.12 (17.95±0.15)
TCB	0.877	26.86	77.16	18.18 (18.05±0.10)

[a]The average PCEs with standard deviations obtained from over 5 independent cells.

References

1. M. J. Frisch, G. W. Trucks, H. B. Schlegel, G. E. Scuseria, M. A. Robb, J. R. Cheeseman, G. Scalmani, V. Barone, G. A. Petersson, H. Nakatsuji, X. Li, M. Caricato, A. V. Marenich, J. Bloino, B. G. Janesko, R. Gomperts, B. Mennucci, H. P. Hratchian, J. V. Ortiz, A. F. Izmaylov, J. L. Sonnenberg, Williams, F. Ding, F. Lipparini, F. Egidi, J. Goings, B. Peng, A. Petrone, T. Henderson, D. Ranasinghe, V. G. Zakrzewski, J. Gao, N. Rega, G. Zheng, W. Liang, M. Hada, M. Ehara, K. Toyota, R. Fukuda, J. Hasegawa, M. Ishida, T. Nakajima, Y. Honda, O. Kitao, H. Nakai, T. Vreven, K. Throssell, J. A. Montgomery Jr., J. E. Peralta, F. Ogliaro, M. J. Bearpark, J. J. Heyd, E. N. Brothers, K. N. Kudin, V. N. Staroverov, T. A. Keith, R. Kobayashi, J. Normand, K. Raghavachari, A. P. Rendell, J. C. Burant, S. S. Iyengar, J. Tomasi, M. Cossi, J. M. Millam, M. Klene, C. Adamo, R. Cammi, J. W. Ochterski, R. L. Martin, K. Morokuma, O. Farkas, J. B. Foresman and D. J. Fox, *Gaussian*, 2016.
2. Q. Xing, F. Xiao, G. Mao and G. J. Deng, *Org. Lett.*, 2022, **24**, 4377-4382.
3. M. Imit, P. Imin and A. Adronov, *Polym. Chem.*, 2016, **7**, 5241-5248.
4. A. Saeki, S. Yoshikawa, M. Tsuji, Y. Koizumi, M. Ide, C. Vijayakumar and S. Seki, *J. Am. Chem. Soc.*, 2012, **134**, 19035-19042.
5. Y. Wang, T. Hasegawa, H. Matsumoto, T. Mori and T. Michinobu, *Adv. Funct. Mater.*, 2017, **27**, 1604608.
6. K. Lu, J. Fang, H. Yan, X. Zhu, Y. Yi and Z. Wei, *Org. Elect.*, 2013, **14**, 2652-2661.
7. W. Yang, W. Wang, Y. Wang, R. Sun, J. Guo, H. Li, M. Shi, J. Guo, Y. Wu, T. Wang, G. Lu, C. J. Brabec, Y. Li and J. Min, *Joule*, 2021, **5**, 1209-1230.
8. T. Lu and F. Chen, *J. Comput. Chem.*, 2012, **33**, 580-592.